Wahlfachpraktikum in der Arbeitsgruppe Elektronenmikroskopie:

SEM & EDX[1]

Scanning Electron Microscopy
and
Energy-dispersive X-ray spectroscopy

Quelle:
R. F. Egerton: Physical Principles of Electron Microscopy, Springer 2005

Online-Zugriff:
`http://dx.doi.org/10.1007/b136495`

[1]Stand: 27. März 2015

Inhalt der Anleitung

Die Anleitung enthält keine Beschreibungen der Versuche, sondern es werden die theoretischen Grundlagen zum Verständnis der durchgeführten Versuche vermittelt. Ähnlich zu den Experimentelle Übungen 2 wird dabei auf vorhandene Literatur zurückgegriffen. Die folgenden Themen werden behandelt:

5. The Scanning Electron Microscope (S. 125 - 137)
    - 5.1 Operating Principle of the SEM
    - 5.2 Penetration of Electrons into a Solid
    - 5.3 Secondary-Electron Images
    - 5.4 Backscattered-Electron Images
6. Analytical Electron Microscopy (S. 158 - 167)
    - 6.2 X-ray Emission Spectroscopy
    - 6.3 X-Ray Energy-Dispersive Spectroscopy
    - 6.4 Quantitative Analysis in the TEM
    - 6.5 Quantitative Analysis in the SEM

Die angegebenen Seitenzahlen beziehen sich auf das Buch **Physical Principles of Electron Microscopy** von Ray F. Egerton in der ersten Auflage von 2005. Die URL zum Buch (Springerlink) ist auf der Titelseite zu finden.

Möglicher Ablauf des Versuch SEM & EDX

Bei diesem Versuch geht es darum die Methode Energy-dispersive X-ray spectroscopy (EDX) kennen zu lernen. Gearbeitet wird an einem Hitachi S-4000. Das Gerät wurde nachträglich mit einem modernen Silicon Drift Detector (SDD) für die Aufzeichnung von Röntgenspektren ausgestattet. Auch eine digitale Ansteuerung inklusive digitaler Bildaufzeichnung wurde nachträglich eingebaut.

Bei der Auswahl der Proben kann auf die Wünsche der Teilnehmer eingegangen werden. Eine Vielzahl von SEM-tauglichen Proben ist vorhanden. Neben diversen Insekten wurden auch Mikrochips, Zähne und vieles mehr für die Untersuchung mit einem SEM vorbereitet. Bei diesen Proben geht es darum ein Gefühl für die Abbildungseigenschaften eines SEM zu bekommen. Es werden deshalb hauptsächlich Bilder aufgenommen.

Für die EDX-Untersuchungen wird auf eine Referenzprobe zurückgegriffen. Diese enthält reine Element, sowie eine Legierung, deren Zusammensetzung bestimmt werden soll. Am Ende dieser Anleitung ist das Datenblatt der Referenzprobe zu finden.

- Untersuchung diverser Proben mit unterschiedlichen Vergrößerungen. Hierbei geht es darum sich die mikroskopische Struktur makroskopischer Objekte anzusehen.

- Spektrometer kalibrieren. Mit Hilfe der reinen Elemente werden Referenzspektren aufgenommen, die für die folgende Quantifizierung genutzt werden.
- Quantifizierung einer Legierung. Mit Hilfe der Referenzspektren soll die Zusammensetzung der Kupferlegierung Messing (engl. Brass) bestimmt werden.

Protokoll

Wir erwarten kein vollständiges Protokoll von euch, so wie es bisher bei den experimentellen Übungen üblich war. Statt dessen reicht ein kurzer Bericht aus. Das bedeutet, dass ihr nicht detailliert auf die theoretischen Grundlagen eingehen sollt. Beim Schreiben des Protokolls könnt ihr davon ausgehen, dass auch der Leser die euch zur Verfügung stehende Literatur kennt und ihr müsst sie deshalb nicht nochmal in eigenen Worten wiedergeben. Die Beschreibung der Versuchsdurchführung und eine kurze Erläuterung der erzielen Ergebnissen ist ausreichend.

Chapter 5

THE SCANNING ELECTRON MICROSCOPE

As we discussed in Chapter 1, the scanning electron microscope (SEM) was invented soon after the TEM but took longer to be developed into a practical tool for scientific research. As happened with the TEM, the spatial resolution of the instrument improved after magnetic lenses were substituted for electrostatic ones and after a stigmator was added to the lens column. Today, scanning electron microscopes outnumber transmission electron microscopes and are used in many fields, including medical and materials research, the semiconductor industry, and forensic-science laboratories.

Figure 1-15 (page 19) shows one example of a commercial high-resolution SEM. Although smaller (and generally less expensive) than a TEM, the SEM incorporates an electron-optical column that operates according to the principles already discussed in Chapter 2 and Chapter 3. Accordingly, our description will be shorter than for the TEM, as we can make use of many of the concepts introduced in these earlier chapters.

5.1 Operating Principle of the SEM

The electron source used in the SEM can be a tungsten filament, or else a LaB_6 or Schottky emitter, or a tungsten field-emission tip. Because the maximum accelerating voltage (typically 30 kV) is lower than for a TEM, the electron gun is smaller, requiring less insulation. Axially-symmetric magnetic lenses are used but they are also smaller than those employed in the TEM; for electrons of lower kinetic energy, the polepieces need not generate such a strong magnetic field. There are also *fewer* lenses; image formation uses the scanning principle that was outlined in Chapter 1, and as a result *imaging lenses* are not required.

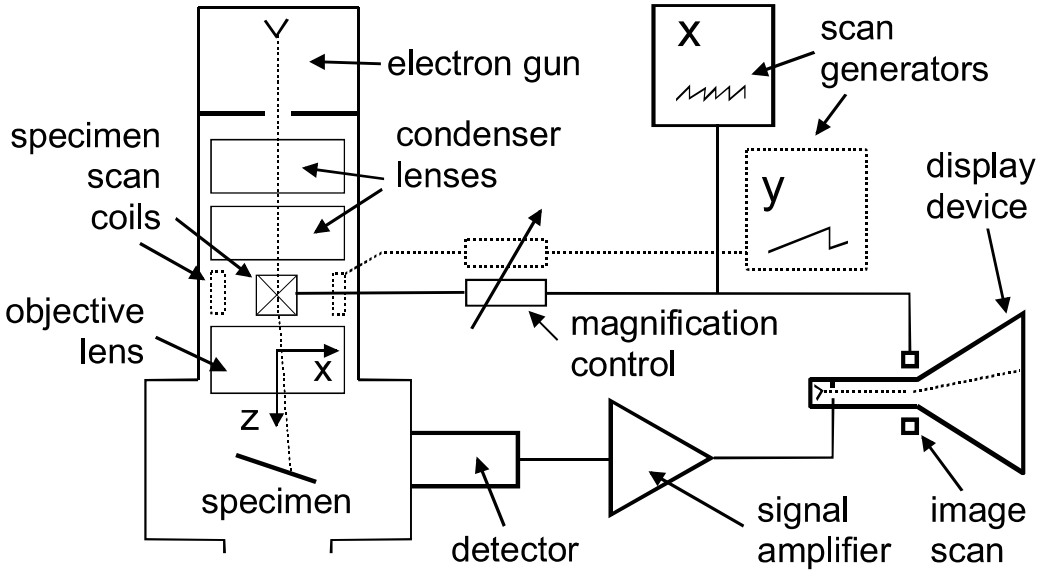

Figure 5-1. Schematic diagram of a scanning electron microscope with a CRT display.

Above the specimen, there are typically two or three lenses, which act somewhat like the condenser lenses of a TEM. But whereas the TEM, if operating in imaging mode, has a beam of diameter ≈ 1 μm or more at the specimen, the incident beam in the SEM (also known as the **electron probe**) needs to be as small as possible: a diameter of 10 nm is typical and 1 nm is possible with a field-emission source. The final lens that forms this very small probe is named the **objective**; its performance (including aberrations) largely determines the spatial resolution of the instrument, as does the objective of a TEM or a light-optical microscope. In fact, the resolution of an SEM can never be better than its incident-probe diameter, as a consequence of the method used to obtain the image.

Whereas the conventional TEM uses a stationary incident beam, the electron probe of an SEM is scanned horizontally across the specimen in two perpendicular (x and y) directions. The x-scan is relatively fast and is generated by a sawtooth-wave generator operating at a **line** frequency f_x; see Fig. 5-2a. This generator supplies scanning current to two coils, connected in series and located on either side of the optic axis, just above the objective lens. The coils generate a magnetic field in the y-direction, creating a force on an electron (traveling in the z-direction) that deflects it in the x-direction; see Fig. 5-1.

The y-scan is much slower (Fig. 5-2b) and is generated by a second sawtooth-wave generator running at a **frame** frequency $f_y = f_x / n$ where n is an integer. The entire procedure is known as **raster scanning** and causes the beam to sequentially cover a rectangular area on the specimen (Fig. 5-2d).

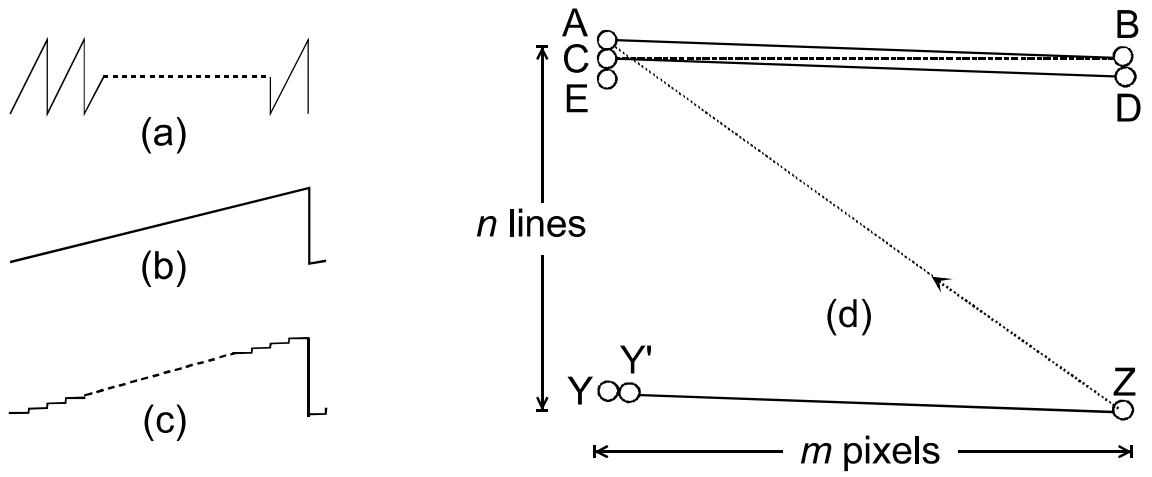

Figure 5-2. (a) Line-scan waveform (scan current versus time),. (b) frame-scan waveform, and (c) its digital equivalent. (d) Elements of a single-frame raster scan: AB and YZ are the first and last line scans in the frame, Y and Y' represent adjacent pixels.

During its *x*-deflection signal, the electron probe moves in a straight line, from A to B in Fig. 5-2d, forming a single **line scan**. After reaching B, the beam is deflected back along the *x*-axis as quickly as possible (the **flyback** portion of the *x*-waveform). But because the *y*-scan generator has increased its output during the line-scan period, it returns *not* to A but to point C , displaced in the *y*-direction. A second line scan takes the probe to point D, at which point it flies back to E and the process is repeated until *n* lines have been scanned and the beam arrives at point Z. This entire sequence constitutes a single **frame** of the raster scan. From point Z, the probe quickly returns to A, as a result of the rapid flyback of *both* the line and frame generators, and the next frame is executed. This process may run continuously for many frames, as happens in TV or video technology.

The outputs of the two scan generators are also applied to a display device, such as a TV-type cathode-ray tube (CRT), on which the SEM image will appear. The electron beam in the CRT scans exactly in *synchronism* with the beam in the SEM, so for every point on the specimen (within the raster-scanned area) there is a *equivalent* point on the display screen, displayed at the same instant of time. Maxwell's first rule of imaging is therefore obeyed (although approximately because the electron beams are not points but circles of small diameter). In order to introduce *contrast* into the image, a voltage signal must be applied to the electron gun of the CRT, to vary the brightness of the scanning spot. This voltage is derived from a detector that responds to *some change in the specimen* induced by the SEM incident probe.

In a modern SEM, the scan signals are generated digitally, by computer-controlled circuitry, and the *x*- and *y*-scan waveforms are actually *staircase*

functions with *m* and *n* levels respectively; see Fig. 5-2c. This procedure divides the image into a total of *mn* picture elements (**pixels**) and the SEM probe remains stationary for a certain dwell time before *jumping* to the next pixel. One advantage of digital scanning is that the SEM computer "knows" the (*x, y*) address of each pixel and can record the appropriate image-intensity value (also as a digitized number) in the corresponding computer-memory location. A digital image, in the form of position and intensity information, can therefore be stored in computer memory, on a magnetic or optical disk, or transmitted over data lines such as the Internet.

Also, the modern SEM uses a flat-panel display screen in which there is no internal electron beam. Instead, computer-generated voltages are used to sequentially define the *x*- and *y*-coordinates of a screen pixel and the SEM detector signal is applied electronically to that pixel, to change its brightness. In other respects, the raster-scanning principle is the same as for a CRT display.

Image magnification in the SEM is achieved by making the *x*- and *y*-scan distances *on the specimen* a small fraction of the size of the displayed image, as by definition the magnification factor *M* is given by:

$$M = (\text{scan distance in the image}) / (\text{scan distance on the specimen}) \quad (5.1)$$

It is convenient to keep the image a *fixed* size, just filling the display screen, so increasing the magnification involves *reducing* the *x*- and *y*-scan currents, each in the same proportion (to avoid image distortion). Consequently, the SEM is actually working hardest (in terms of current drawn from the scan generator) when operated at *low* magnification.

The scanning is sometimes done at video rate (about 60 frames/second) to generate a rapidly-refreshed image that is useful for focusing the specimen or for viewing it at low magnification. At higher magnification, or when making a permanent record of an image, slow scanning (several seconds per frame) is preferred; the additional recording time results in a higher-quality image containing less electronic noise.

The signal that modulates (alters) the image brightness can be derived from any property of the specimen that changes in response to electron bombardment. Most commonly, the emission of **secondary electrons** (atomic electrons ejected from the specimen as a result of inelastic scattering) is used. However, a signal derived from **backscattered electrons** (incident electrons elastically scattered through more than 90 degrees) is also useful. In order to understand these (and other) possibilities, we need to

consider what happens when an electron beam enters a *thick* (often called bulk) specimen.

5.2 Penetration of Electrons into a Solid

When accelerated electrons enter a solid, they are scattered both *elastically* (by electrostatic interaction with atomic nuclei) and *inelastically* (by interaction with atomic electrons), as already discussed in Chapter 4. Most of this interaction is "forward" scattering, which implies deflection angles of less than 90°. But a small fraction of the primaries are elastically backscattered ($\theta > 90°$) with only small fractional loss of energy. Due to their high kinetic energy, these backscattered electrons have a reasonable probability of leaving the specimen and re-entering the surrounding vacuum, in which case they can be collected as a backscattered-electron (**BSE**) signal.

Inelastic scattering involves relatively small scattering angles and so contributes little to the backscattered signal. However, it reduces the kinetic energy of the primary electrons until they are eventually brought to rest and absorbed into the solid; in a metal specimen they could become conduction electrons. The depth (below the surface) at which this occurs is called the **penetration depth** or the **electron range**. The volume of sample containing (most of) the scattered electrons is called the **interaction volume** and is often represented as pear-shaped in cross section (Fig. 5-3), because scattering causes the beam to spread laterally as the electrons penetrate the solid and gradually lose energy.

The electron range R for electrons of incident energy E_0 is given by the following approximate formula (Reimer 1998):

$$\rho R \approx a\, E_0^{\,\mathrm{r}} \tag{5.2}$$

where $b \approx 1.35$ and ρ is the density of the specimen. If E_0 is given *in keV* in Eq. (5.2), $a \approx 10$ μg/cm^2. Expressing the range as a **mass-thickness** ρR makes the coefficient a roughly independent of atomic number Z. However, this implies that the distance R itself decreases with Z, as the densities of solids tend to increase with atomic number. For carbon ($Z = 6$), $\rho \approx 2$ g/cm^3 and $R \approx 1$ μm for a 10-keV electron. But for gold ($Z = 79$), $\rho \approx 20$ g/cm^3 and $R \approx 0.2$ μm at $E_0 = 10$ keV. This strong Z-dependence arises mainly because backscattering depletes the number of electrons moving forward into the solid, the probability of such high-angle elastic scattering being proportional to Z^2, as seen from Eq. (4.15). The interaction volume is therefore smaller for materials of higher atomic number (Fig. 5-3).

According to Eq. (5.2), the range decreases substantially with decreasing incident energy, not surprising because lower-energy electrons require fewer

inelastic collisions to bring them to rest and also the probability of inelastic scattering is inversely proportional to E_0. A 1-keV electron penetrates only about 50 nm into carbon and less than 10 nm into gold. The interaction volume therefore becomes very small at low incident energy; see Fig. 5-3.

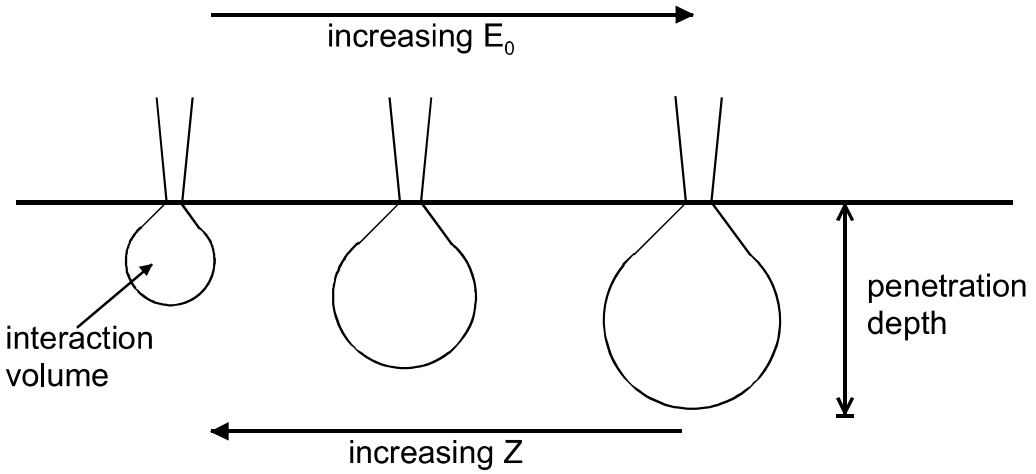

Figure 5-3. Schematic dependence of the interaction volume and penetration depth as a function of incident energy E_0 and atomic number Z of the incident (primary) electrons.

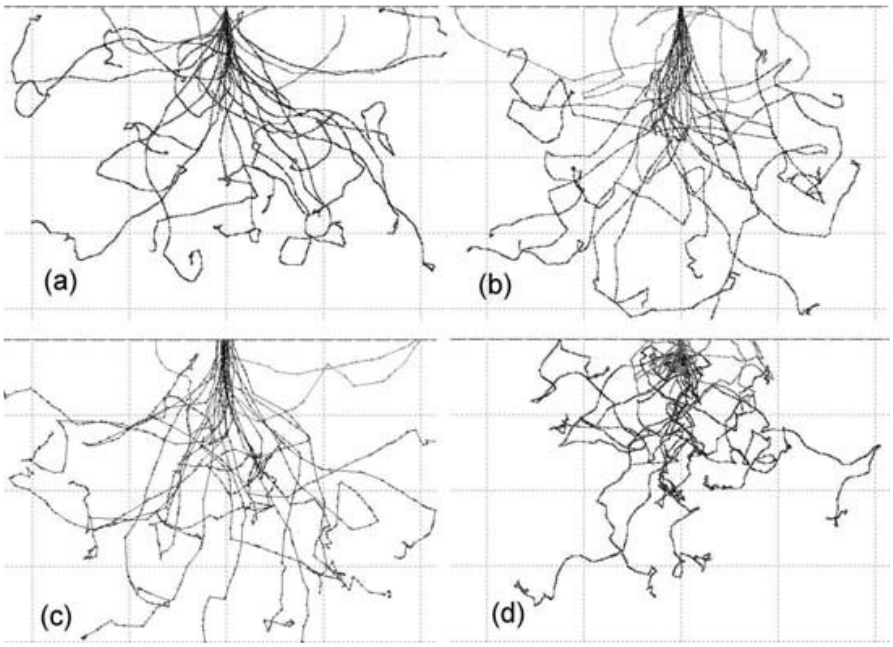

Figure 5-4. Penetration of (a) 30-keV, (b) 10-keV and (c) 3-keV electrons into aluminum (Z = 13) and (d) 30-keV electrons into gold (Z = 79). Note that the dimensional scales are different: the maximum penetration is about 6.4 μm, 0.8 μm, and 0.12 μm in (a), (b), and (c), and 1.2 μm in (d). These Monte Carlo simulations were carried out using the CASINO program (Gauvin et al., 2001) with 25 primary electrons and an incident-beam diameter equal to 10 nm in each case.

Penetration depth and interaction volume are macroscopic quantities, averaged over a large number of electrons, but the behavior of an *individual* electron is highly variable. In other words, scattering is a statistical process. It can be simulated in a computer by running a Monte Carlo program that contains a random-number generator and information about the angular distributions of elastic and inelastic scattering. Figure 5-4 shows the trajectories of 25 primary electrons entering both aluminum and gold. Sudden changes in direction represent the elastic or inelastic scattering. Although the behavior of each electron is different, the very dissimilar length scales needed to represent the different values of E_0 and Z in Fig. 5-4 are a further illustration of the overall trends represented by Eq. (5.2).

5.3 Secondary-Electron Images

From the principle of conservation of energy, we know that any energy *lost* by a primary electron will appear as a *gain* in energy of the atomic electrons that are responsible for the inelastic scattering. If these are the outer-shell (valence or conduction) electrons, weakly bound (electrostatically) to an atomic nucleus, only a small part of this acquired energy will be used up as potential energy, to release them from the confines of a particular atom. The remainder will be retained as kinetic energy, allowing the escaping electrons to travel through the solid as secondary electrons (abbreviated to **SE** or **secondaries**). As moving charged particles, the secondaries themselves will interact with other atomic electrons and be scattered inelastically, gradually losing their kinetic energy. In fact, most SEs start with a kinetic energy of less than 100 eV and, because the probability of inelastic scattering depends *inversely* on kinetic energy as in Eq. (4.16), the average distance that a secondary travels in the solid is very small, typically one or two nm.

As a result, most secondaries are brought to rest *within* the interaction volume. But those created close to the surface may escape into the vacuum, especially if they are initially traveling *toward* the surface. On average, the *escaping* secondaries are generated only within very small depth (< 2 nm) below the surface, called the **escape depth**. Because the SE signal used in the SEM is derived from secondaries that escape into the vacuum, the SE image is a property of the *surface structure* (topography) of the specimen rather than any underlying structure; the image is said to display **topographical contrast**.

The average number of *escaping* secondaries *per primary electron* is called the **secondary-electron yield**, δ, and is typically in the range from 0.1 to 10; the exact value depends on the chemical composition of the specimen

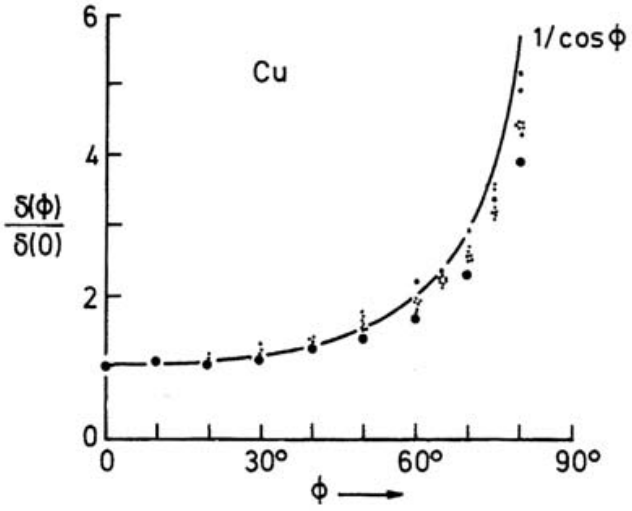

Figure 5-5. Dependence of SE yield on the angle of tilt φ of the specimen, measured between a plane perpendicular to its surface and the primary-electron beam (φ = 0 corresponds to normal incidence). Data points represent experimental measurements and Monte Carlo predictions for copper; the curve represents a $1/\cos\varphi$ function. From Reimer (1998), courtesy of Springer-Verlag.

(close to the surface) and on the primary-electron energy E_0. For a given specimen, δ decreases with increasing E_0 because higher-energy primaries undergo less inelastic scattering (per unit distance traveled) and so there will be fewer secondaries generated *within the escape depth*.

As Fig. 5-5 indicates, the secondary-electron yield also depends on the angle between the incoming primary electron and the surface. The yield is lowest for normal (perpendicular) incidence and increases with increasing angle between the primary beam and the surface-normal. The reason is illustrated in Fig. 5-6a, which shows a focused nearly-parallel beam of primary electrons (diameter d) incident at two locations on a specimen, where the surface is normal (at A) and inclined (at B) to the incident beam. The region from which secondary electrons can escape is such that all points within it lie within the escape depth λ of the surface. For normal incidence, this escape region is a cylinder of radius $d/2$, height λ and volume $V(0) = (\pi/4)\,d^2\lambda$. For the inclined surface, the escape region is a slanted cylinder with height λ (perpendicular to the surface) and base of cross-sectional area $(\pi/4)(d/\cos\phi)^2$, giving escape volume $V(\phi) = \pi(d/2)^2(\lambda/\cos\phi) = V(0)/\cos\phi$. Because the SE yield is proportional to the number of SE generated within the escape region, δ is proportional to the escape volume, resulting in:

$$\delta(\phi) = \delta(0)/\cos\phi \qquad (5.3)$$

Measurements of $\delta(\phi)$ support this inverse-cosine formula; see Fig. 5-5.

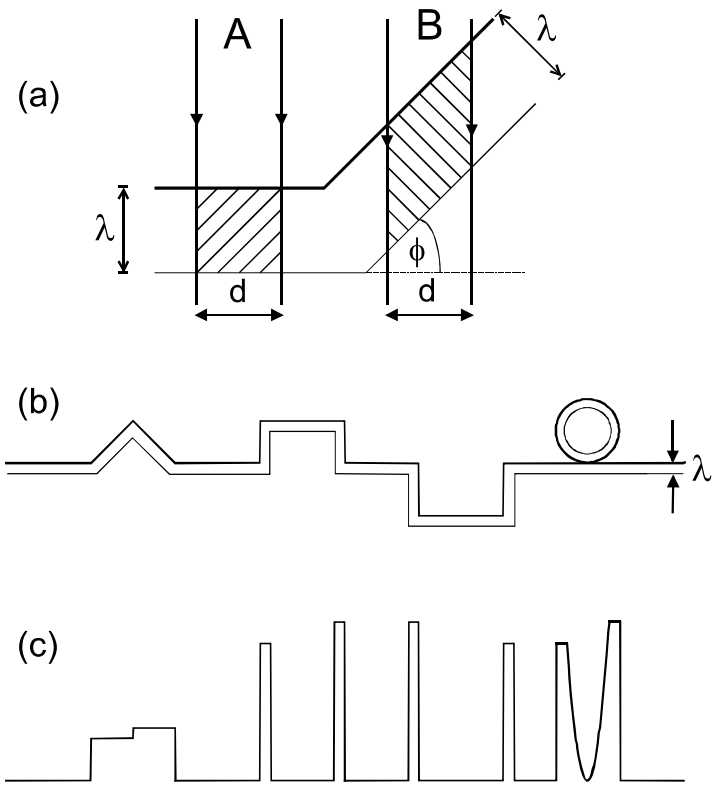

Figure 5-6. (a) SEM incident beam that is normal to a specimen surface (at A) and inclined to the surface (at B). The volume from which secondaries can escape is proportional to the shaded cross-sectional area, which is λd for case A and $\lambda d/\cos\phi$ for a tilted surface (case B). (b) Cross-sectional diagram of a specimen surface that contains triangular and square protrusions, a square-shaped trough or well, and a spherical particle; λ is the SE escape depth. (c) Corresponding secondary-electron signal (from a line-scan along the surface), assuming a SE detector that is located to the right of the specimen.

In qualitative terms, non-normal irradiation of a surface generates more SE that lie within a *perpendicular* distance λ of the surface and can therefore escape into the vacuum. For a surface with topographical (height) variations (Fig. 5-6b), this orientation dependence of δ results in protruding or recessed features appearing *bright in outline* in the SE image (Figs. 5-6c and 5-7a), similar to thickness-gradient contrast from a TEM replica.

In practice, there is usually some asymmetry due to the fact that the SE detector is located to one side of the column (Fig. 5-1) rather than directly above. Surface features that are tilted *toward* the detector appear especially bright because electrons emitted from these regions have a greater probability of reaching the detector; see Fig. 5-7a. This fact can be used to *distinguish* raised features and depressions in the surface of the specimen, as illustrated in Fig. 5-6c. As a result, the SE image has a three-dimensional appearance, similar to that of a rough surface obliquely illuminated by light, which makes the topographical contrast relatively easy to interpret; see also Fig. 5-9a.

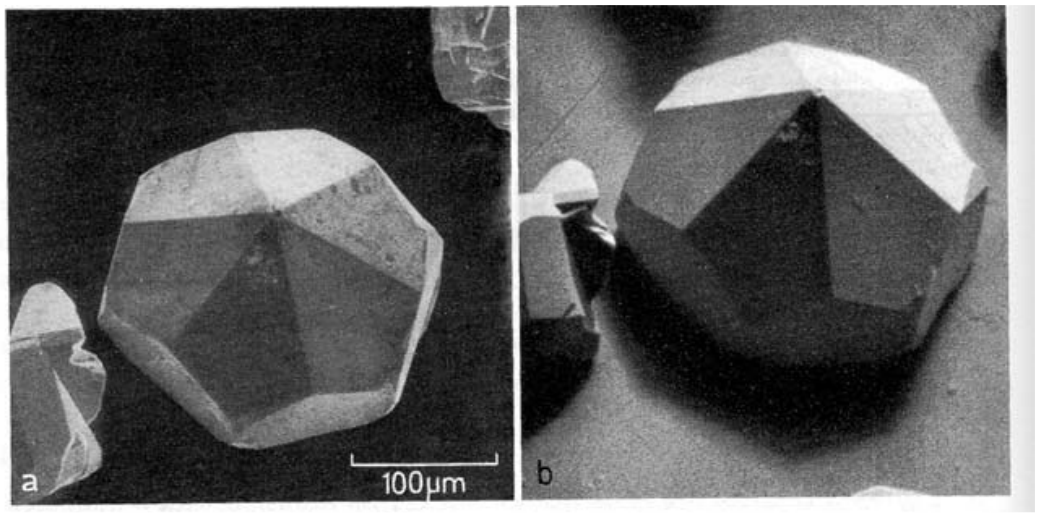

Figure 5-7. (a) Secondary-electron image of a small crystal; the side-mounted Everhart-Thornley detector is located toward the top of the image. (b) Backscattered-electron image recorded by the same side-mounted detector, which also shows topographical contrast and shadowing effects. Such contrast is much weaker for a BSE detector mounted directly above the specimen. From Reimer (1998), courtesy of Springer-Verlag.

Taking advantage of the orientation dependence of δ, the *whole sample* is often tilted away from a horizontal plane and toward the detector, as shown in Fig. 5-1. This increases the overall SE signal, averaged over all regions of the sample, while preserving the topographic contrast due to *differences* in surface orientation.

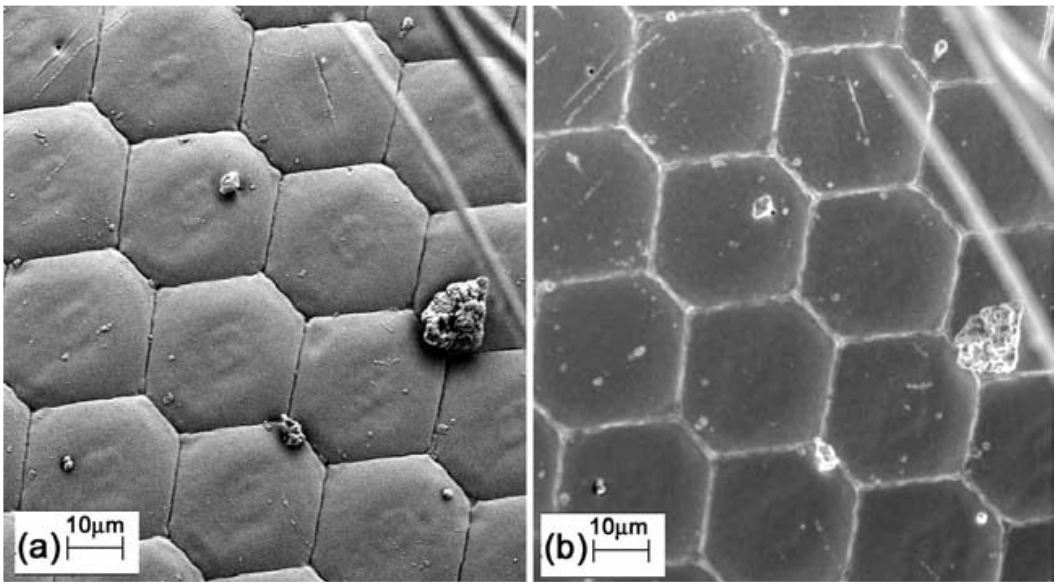

Figure 5-9. Compound eye of an insect, coated with gold to make the specimen conducting. (a) SE image recorded by a side-mounted detector (located toward the top of the page) and showing a strong directional effect, including dark shadows visible below each dust particle. (b) SE image recorded by an in-lens detector, showing topographical contrast but very little directional or shadowing effect. Courtesy of Peng Li, University of Alberta.

5.4 Backscattered-Electron Images

A backscattered electron (BSE) is a primary electron that has been ejected from a solid by scattering through an angle greater than 90 degrees. Such deflection could occur as a result of several collisions, some or all of which might involve a scattering angle of *less* than 90 degrees; however, a *single* elastic event with $\theta > 90$ degrees is quite probable. Because the elastic scattering involves only a *small* energy exchange, most BSEs escape from the sample with energies not too far below the primary-beam energy; see Fig. 5-10. The secondary and backscattered electrons can therefore be distinguished on the basis of their kinetic energy.

Because the cross section for high-angle elastic scattering is proportional to Z^2, we might expect to obtain strong *atomic-number* contrast by using backscattered electrons as the signal used to modulate the SEM-image intensity. In practice, the **backscattering coefficient** η (the fraction of primary electrons that escape as BSE) *does* increase with atomic number, (almost linearly for low Z), and BSE images can show contrast due to variations in chemical composition of a specimen, whereas SE images reflect mainly its surface topography.

Another difference between the two kinds of image is the *depth* from which the information originates. In the case of a BSE image, the signal comes from a depth of up to about *half* the penetration depth (after being generated, each BSE must have enough energy to get out of the solid). For primary energies above 3 kV, this means some *tens or hundreds* of nanometers rather than the much smaller SE escape depth ($\approx$ 1 nm).

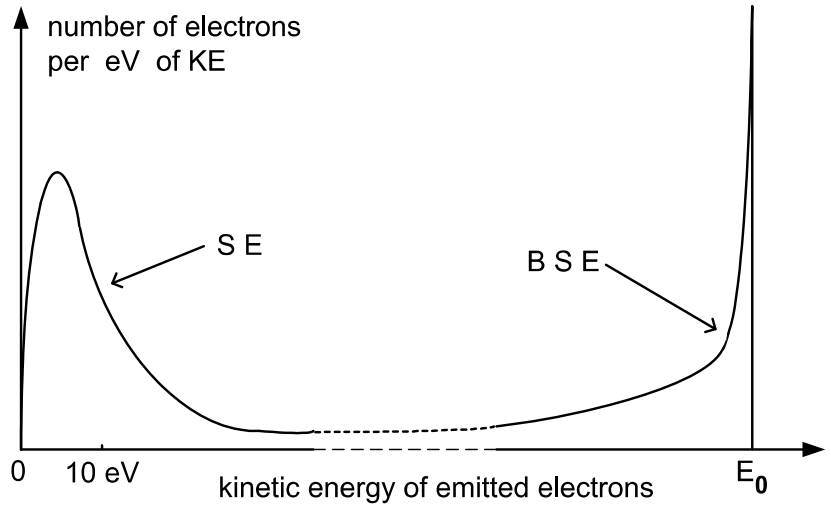

Figure 5-10. Number of electrons emitted from the SEM specimen as a function of their kinetic energy, illustrating the conventional classification into secondary and backscattered components.

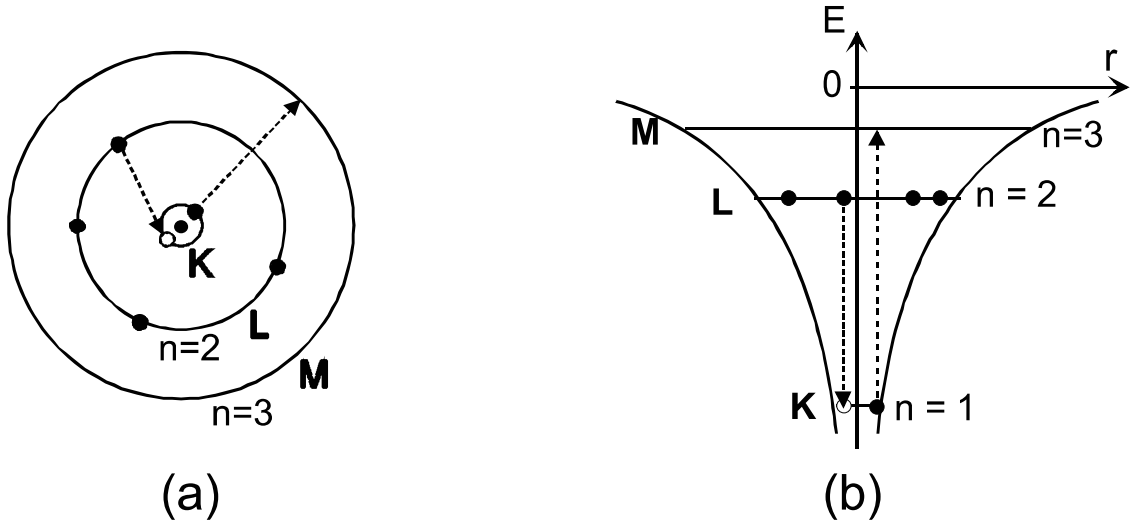

Figure 6-1. Bohr model of a carbon atom, visualized in terms of (a) electron orbits and (b) the equivalent energy levels. The orbits are also described as electron shells and are designated as K (n = 1), L (n = 2), M (n = 3) and so forth. The dashed arrows illustrate a possible scenario for x-ray emission: a K-shell electron (n_l = 1) is excited to the empty M-shell (n_u = 3) and an L-shell electron fills the K-shell vacancy in a de-excitation process (n_l = 1, n_u =2).

$$hf = -R\,Z^2/n_u^2 - (-R\,Z^2/n_l^2) = RZ^2(1/n_l^2 - 1/n_u^2) \qquad (6.5)$$

6.2 X-ray Emission Spectroscopy

When a primary electron enters a TEM or SEM specimen, it has a (small) probability of being scattered inelastically by an *inner-shell* (e.g. K-shell) electron, causing the latter to undergo a transition to a higher-energy orbit (or wave-mechanical state) and leaving the atom with an electron vacancy (hole) in its inner shell. However, the scattering atom remains in this *excited* state for only a very brief period of time: within about 10^{-15} s, one of the other atomic electrons fills the inner-shell vacancy by making a *downward* transition from a higher energy level, as in Fig. 6-1b. In this de-excitation process, energy can be released in the form of a *photon* whose energy (hf) is given roughly by Eq. (6.5) but more accurately by the *actual* difference in binding energy between the upper and lower levels.

The energy of this **characteristic x-ray** photon therefore depends on the atomic number Z of the atom involved and on the quantum numbers (n_l, n_u) of the energy levels involved in the electron transition. Characteristic x-rays can be classified according to the following historical scheme. The electron shell in which the original inner-shell vacancy was created, which corresponds to the quantum number n_l, is represented by an upper-case

letter; thus K implies that $n_l = 1$, L implies $n_l = 1$, M implies $n_l = 1$ and so on. This Roman symbol is followed by a Greek letter that represents the *change in* quantum number: α denotes $(n_u - n_l) = 1$, β denotes $(n_u - n_l) = 2$, and γ denotes $(n_u - n_l) = 3$. Sometimes a numerical subscript is added to allow for the fact that some energy levels are split into components of slightly different energy, due to quantum-mechanical effects.

The transition sequence represented in Fig. 6-1b would therefore result in a Kα x-ray being emitted, and in the case of carbon there is no other possibility. With an atom of higher atomic number, containing electrons in its M-shell, an M- to K-shell transition would result in a Kβ x-ray (of greater energy) being emitted. Similarly, a vacancy created (by inelastic scattering of a primary electron) in the L-shell might result in emission of an Lα photon. These possibilities are illustrated in Fig. 6-2, which shows the x-ray emission spectrum recorded from a TEM specimen consisting of a thin film of nickel oxide (NiO) deposited onto a thin carbon film and supported on a molybdenum (Mo) TEM grid.

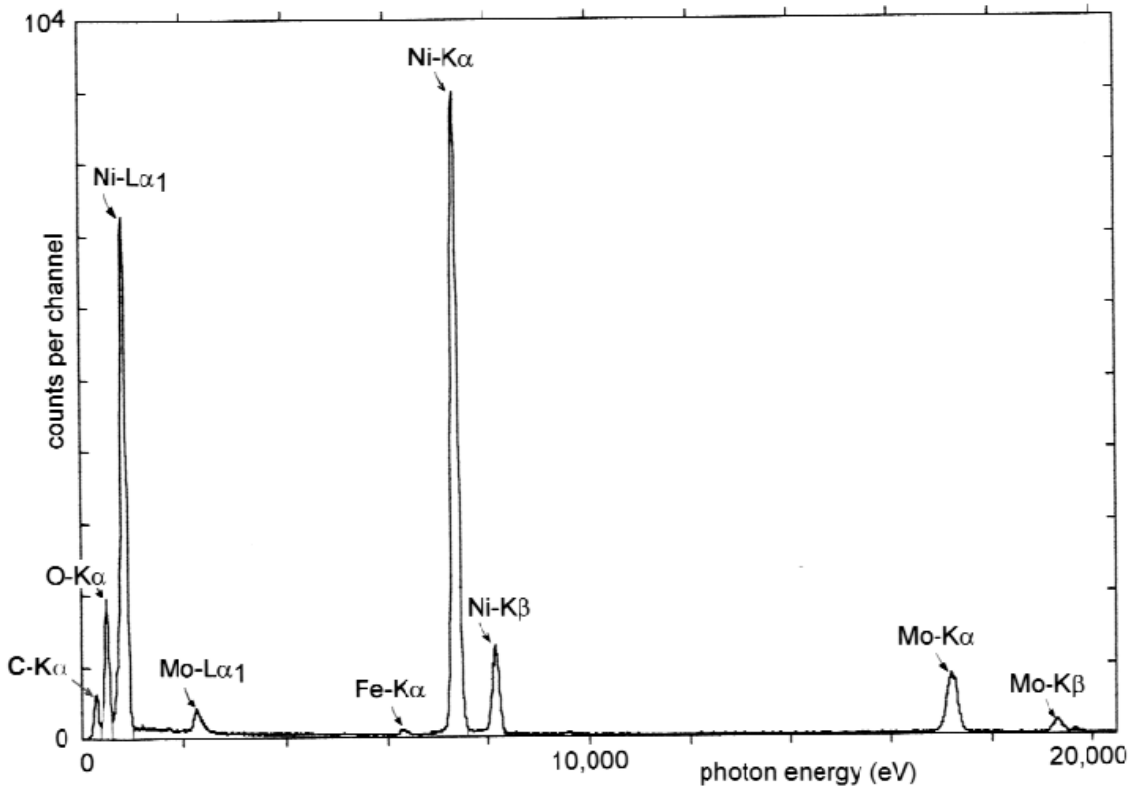

Figure 6-2. X-ray emission spectrum (number of x-ray photons as a function of photon energy) recorded from a TEM specimen (NiO thin film on a Mo grid), showing characteristic peaks due to the elements C, O, Ni, Mo, and Fe. For Ni and Mo, both K- and L-peaks are visible. Mo peaks arise from the grid material; the weak Fe peak is from the TEM polepieces.

Figure 6-2 also demonstrates some general features of x-ray emission spectroscopy. First, each element gives rise to *at least one* characteristic peak and can be identified from the photon energy associated with this peak. Second, medium- and high-Z elements show *several* peaks (K, L, etc.); this complicates the spectrum but can be useful for multi-element specimens where some characteristic peaks may overlap with each other, making the measurement of elemental concentrations problematical if based on only a single peak per element. Third, there are always a few stray electrons outside the focused electron probe (due to spherical aberration, for example), so the x-ray spectrum contains contributions from elements in the nearby environment, such as the TEM support grid or objective-lens polepieces.

High-Z atoms contain a large number of electron shells and can in principle give rise to *many* characteristic peaks. In practice, the number is reduced by the need to satisfy conservation of energy. As an example, gold (Z = 79) has its K-emission peaks above 77 keV, so in an SEM, where the primary-electron energy is rarely above 30 keV, the primary electrons do not have enough energy to excite K-peaks in the x-ray spectrum.

The characteristic peaks in the x-ray emission spectrum are superimposed on a continuous background that arises from the **bremsstrahlung** process (German for braking radiation, implying deceleration of the electron). If a primary electron passes close to an atomic nucleus, it is elastically scattered and follows a curved (hyperbolic) trajectory, as discussed in Chapter 4. During its deflection, the electron experiences a Coulomb force and a resulting centripetal acceleration toward the nucleus. Being a charged particle, it must emit electromagnetic radiation, with an amount of energy that depends on the impact parameter of the electron. The latter is a *continuous* variable, slightly different for each primary electron, so the photons emitted have a broad range of energy and form a background to the characteristic peaks in the x-ray emission spectrum. In Fig. 6-2, this bremsstrahlung background is low but is visible between the characteristic peaks at low photon energies.

Either a TEM or an SEM can be used as the means of generating an x-ray emission spectrum from a small region of a specimen. The SEM uses a thick (bulk) specimen, into which the electrons may penetrate several micrometers (at an accelerating voltage of 30 kV), so the x-ray intensity is higher than that obtained from the thin specimen used in a TEM. In both kinds of instrument, the volume of specimen emitting x-rays depends on the *diameter* of the primary beam, which can be made very small by focusing the beam into a probe of diameter 10 nm or less. In the case of the TEM, where the sample is thin and lateral spread of the beam (due to elastic scattering) is limited, the analyzed volume can be as small as 10^{-19} cm^2, allowing detection

of less than 10^{-19} g of an element. In the SEM, x-rays are emitted from the entire interaction volume, which becomes larger as the incident energy of the electrons is increased (Fig. 5-3).

To generate a spectrum from the emitted x-rays, we need some form of *dispersive* device that distinguishes x-ray photons on the basis of either their energy ($E = hf$, where f is the frequency of the electromagnetic wave) or their wavelength ($\lambda = c/f = hc/E$, where c is the speed of light in vacuum). Although photon energy and wavelength are closely related, these two options give rise to two distinct forms of spectroscopy, which we discuss in Sections 6.3 and 6.6.

6.3 X-ray Energy-Dispersive Spectroscopy

In x-ray energy-dispersive spectroscopy (XEDS), the dispersive device is a semiconductor diode, fabricated from a single crystal of silicon (or germanium) and somewhat similar to the BSE detector in an SEM. If an x-ray photon enters and penetrates to the transition region (between p- and n-doped material), its energy can release a considerable number of outer-shell (valence) electrons from the confinement of a particular atomic nucleus. This process is equivalent to exciting electrons from the valence to the conduction band (i.e,. the creation of electron-hole pairs) and results in electrical conduction by both electrons and holes for a brief period of time. With a reverse-bias voltage applied to the diode, this conduction causes electrical charge to flow through the junction (and around an external circuit), the charge being proportional to the number N of electron-hole pairs generated. Assuming that all of the photon energy (hf) goes into creating electron-hole (e-h) pairs, each pair requiring an average energy ΔE, energy conservation implies:

$$N = hf/\Delta E \tag{6.6}$$

For silicon, $\Delta E \approx 4$ eV (just over *twice* the energy gap between valence and conduction bands), therefore a Cu-Kα photon creates about (8000eV)/(4eV) = 2000 e-h pairs.

To ensure that essentially *all* of the incoming x-rays are absorbed and generate current pulses in an external circuit, the p-n transition region is made much *wider* than in most semiconductor diodes. In the case of silicon, this can be done by diffusing in the element lithium (Z = 3), which annihilates the effect of other electrically-active (dopant) impurities and creates a high-resistivity (intrinsic) region several mm in width; see Fig. 6-3.

If the semiconductor diode were operated at room temperature, *thermal* generation of electron-hole pairs would contribute too much electronic noise

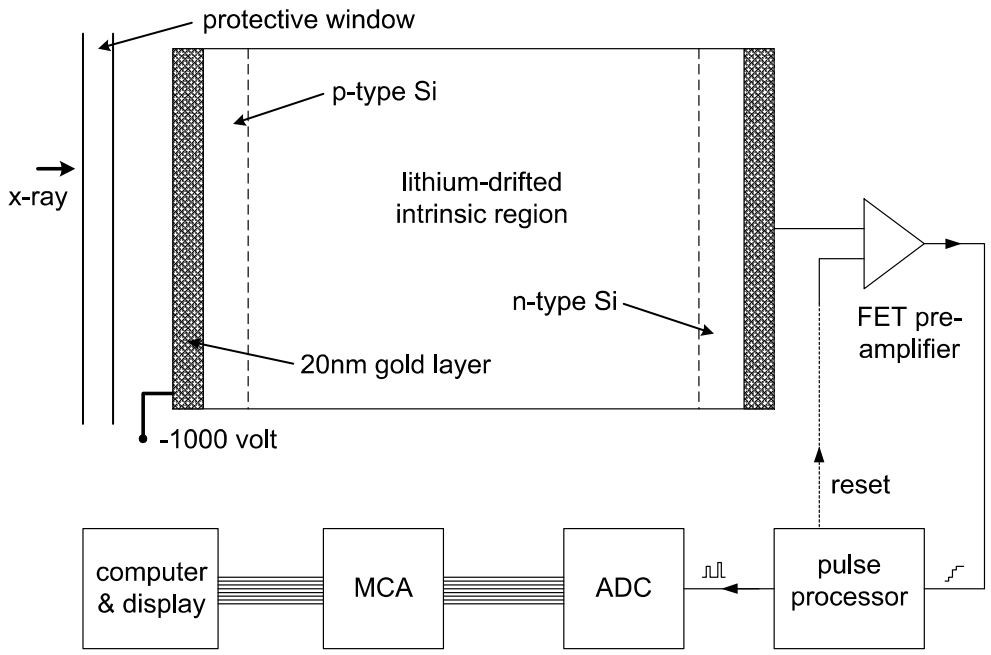

Figure 6-3. Schematic diagram of a XEDS detector and its signal-processing circuitry.

to the x-ray spectrum. Therefore the diode is cooled to about 140 K, via a metal rod that has good thermal contact with an insulated (dewar) vessel containing liquid nitrogen at 77 K. To prevent water vapor and hydrocarbon molecules (present at low concentration in an SEM or TEM vacuum) from condensing onto the cooled diode, a thin protective window precedes the diode; see Fig. 6-3. Originally this window was a thin (≈ 8 μm) layer of beryllium, which because of its low atomic number ($Z = 4$) transmits most x-rays without absorption. More recently, ultra-thin windows (also of low-Z materials, such as diamond or boron nitride) are used to minimize the absorption of low-energy (< 1 keV) photons and allow the XEDS system to analyze elements of low atomic number ($Z < 12$) via their K-emission peaks.

The current pulses from the detector crystal are fed into a field-effect transistor (FET) preamplifier located just behind the diode (see Fig. 6-3) and also cooled to reduce electronic noise. For noise-related reasons, the FET acts as a *charge-integrating* amplifier: for each photon absorbed, its output voltage increases by an amount that is proportional to its input, which is proportional to N and , according to Eq. (6.6), to the photon energy. The output of the FET is therefore a *staircase* waveform (Fig. 6-4a) with the height of each step proportional to the corresponding photon energy. Before the FET output reaches its saturation level (above which the FET would no longer respond to its input), the voltage is reset to zero by applying an electrical (or optical) trigger signal to the FET.

A pulse-processing circuit (Fig. 6-3) converts each voltage step into a signal *pulse* whose height is proportional to the voltage step and which is therefore proportional to the photon energy; see Fig. 6-4b. An analog-to-digital converter (ADC) then produces a sequence of constant-height pulses from each signal pulse (Fig. 6-4c), their number being proportional to the input-pulse height. This procedure is called **pulse-height analysis** (PHA) and is also used in particle-physics instrumentation. Finally, a **multichannel analyzer** (MCA) circuit counts the number (n) of pulses in each ADC-output sequence and increments (by one count) the number stored at the n'th location (address) of a computer-memory bank, signifying the recording of a photon whose energy is proportional to n, and therefore to N and to photon energy. At frequent time intervals (such as 1 s), the computer-memory contents are read out as a spectrum display (Fig. 6-4d) in which the horizontal axis represents photon energy and the vertical scale represents the number of photons counted at that energy.

Typically, the spectrum contains $2^{12} = 4096$ memory locations (known as channels) and each channel corresponds to a 10 eV range of photon energy, in which case the entire spectrum extends from zero and just over 40 keV, sufficient to include almost all the characteristic x-rays. Because the number N of electron-hole pairs produced in the detector is subject to a statistical variation, each characteristic peak has a width of *several* channels. The peaks therefore appear to have a smooth (Gaussian) profile, centered around the characteristic photon energy but with a width of ≈ 150 eV, as in Fig. 6-2.

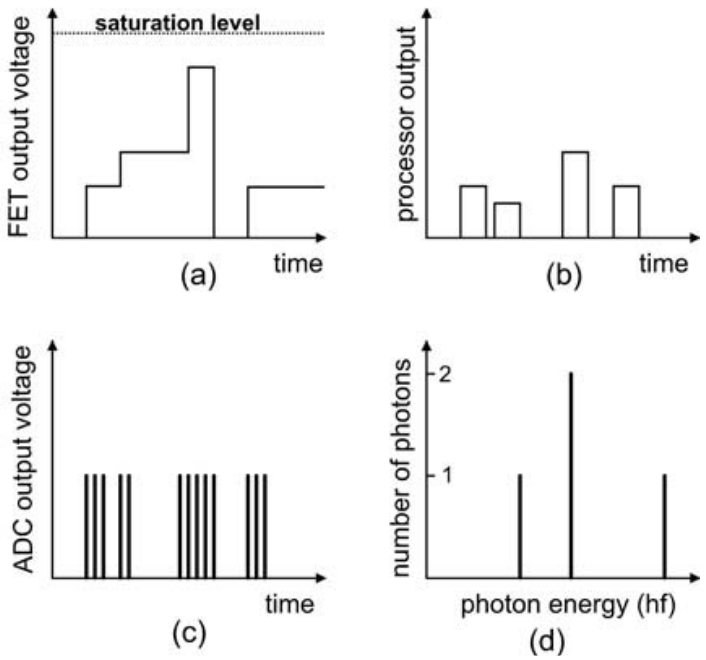

Figure 6-4. Voltage output signals of (a) the FET preamplifer, (b) the pulse-processor circuit, and (c) the analog-to-digital converter (ADC), resulting in (d) the XEDS-spectrum display.

Ideally, each peak in the XEDS spectrum represents an element present *within a known region of the specimen*, defined by the focused probe. In practice, there are often additional peaks due to elements beyond that region or even outside the specimen. Electrons that are backscattered (or in a TEM, forward-scattered through a large angle) strike objects (lens polepieces, parts of the specimen holder) in the immediate vicinity of the specimen and generate x-rays that are characteristic of those objects. Fe and Cu peaks can be produced in this way. In the case of the TEM, a special "analytical" specimen holder is used whose tip (surrounding the specimen) is made from beryllium (Z = 4), which generates a single K-emission peak at an energy below what is detectable by most XEDS systems. Also, the TEM objective aperture is usually removed during x-ray spectroscopy, to avoid generating backscattered electrons at the aperture, which would bombard the specimen from below and produce x-rays far from the focused probe. Even so, spurious peaks sometimes appear, generated from thick regions at the edge a thinned specimen or by a specimen-support grid. Therefore, caution has to be used in interpreting the significance of the x-ray peaks.

It takes a certain period of time (conversion time) for the PHA circuitry to analyze the height of each pulse. Because x-ray photons enter the detector at random times, there is a certain probability of another x-ray photon arriving within this conversion time. To avoid generating a false reading, the PHA circuit ignores such double events, whose occurrence increases as the photon-arrival rate increases. A given recording time therefore consists of two components: **live time**, during which the system is processing data, and **dead time**, during which the circuitry is made inactive. The beam current in the TEM or SEM should be kept low enough to ensure that the dead time is less than the live time, otherwise the number of photons *measured* in a given recording time starts to fall; see Fig. 6-5.

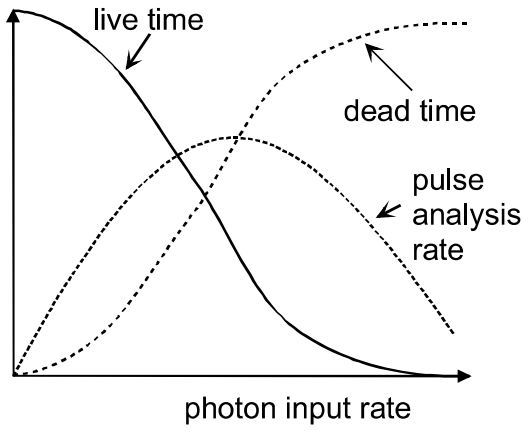

Figure 6-5. Live time, dead time, and pulse-analysis rate, as a function of the generation rate of x-rays in the specimen.

The time taken to record a useful XEDS spectrum is dictated by the need to clearly identify the *position* of each significant peak (its characteristic energy) and also, for measurement of elemental ratios, the *total number of photon counts* in each peak (the peak integral or area). If the recording time is too short, an insufficient number of x-ray photons will be analyzed and the spectrum will be "noisy." This electronic noise arises from the fact that the generation of x-rays in the specimen is a statistical process, giving rise to a statistical variation in the number of counts per channel in the XEDS spectrum. According to the rules of (Poisson) statistics, if N randomly-arriving photons are recorded, we can expect a *variation* in that number (the standard deviation) equal to $N^{1/2}$ if the experiment were repeated many times. The accuracy of measuring N is therefore $N^{1/2}$ and the fractional accuracy is $N^{1/2}/N = N^{-1/2} = 0.1$ for $N = 100$. As a result, we need *at least* 100 x-ray counts in a characteristic peak in order to measure the concentration of the corresponding element to an accuracy of 10%. Typically, this condition implies a recording time of at least 10 s, and sometimes several minutes if the x-ray generation rate is low (e.g., with a thin specimen in the TEM).

One important feature of XEDS analysis is that it can provide a *quantitative* estimate of the concentration ratios of elements present in a specimen. The first requirement is to determine the number of characteristic x-ray photons contributing to each peak, by measuring the area (integral) of the peak and subtracting a contribution from the bremsstrahlung background. This background contribution is estimated by measuring the background on either side of the peak, then interpolating or (for greater accuracy) fitting the background to some simple mathematical function. However, the ratio of two peak integrals is *not* equal to the ratio of the elemental concentrations, as x-rays are not emitted with equal efficiency by different elements. The physics of x-ray production is simplest for the case of a very *thin* specimen, as used in the TEM, so we consider this situation first.

6.4 Quantitative Analysis in the TEM

For quantification, we need an equation that relates the number N_A of x-ray photons contributing to a characteristic peak of an element A to its concentration n_A (number of atoms of element A per unit volume). We can expect N_A to be proportional to the number N_e of electrons that pass through the sample during the XEDS recording time, and to the product $n_A t$, where t is the specimen thickness (for thin specimens, the probability of inner-shell inelastic scattering increases proportional to t).

However, the product $n_A t$ (termed the areal density of the element) has dimensions of m^{-2}, whereas N_A and N_e are dimensionless numbers. In order

to balance the units in our equation, there must be an additional factor whose dimensions are m^2. This factor is the **ionization cross section** σ_A for creating a vacancy in an *inner shell* of element A. Such a cross section can be interpreted as a *target area* for inelastic scattering of an incident electron by the atom, as discussed Section 4.3. The value of σ_A depends on the type of inner shell (K, L, etc.) as well as on the atomic number of the element.

Still missing from our equation is a factor known as the **fluorescence yield** that allows for the fact that not *every* inner-shell vacancy gives rise to the emission of an x-ray photon during the de-excitation of the atom. An alternative process allows the excited atom to return to its ground state by donating energy to another electron within the atom, which is ejected as an **Auger electron** (named after its discoverer, Pierre Auger). For elements of low atomic number, this Auger process is the more probable outcome and their *x-ray* fluorescence yield ω is considerably less than one ($\omega << 1.0$).

A remaining factor, known as the **collection efficiency,** η, of the XEDS detector, reflects the fact that x-ray photons are emitted equally in all directions; they travel in straight-line paths and only a fraction η of them reach the detector. Combining all of these factors, the number of x-ray photons contributing to the characteristic peak of an element A is

$$N_A = (n_A\, t)\, \sigma_A\, \omega_A\, \eta\, N_e \tag{6.7}$$

Applying the same considerations to some other element B present in the sample, we could generate a second equation, identical to Eq. (6.7) but with subscripts B. Dividing Eq. (6.7) by this second equation, we obtain an expression for the *concentration ratio* of the two elements:

$$n_A/n_B = [(\sigma_B\, \omega_B)/(\sigma_A\, \omega_A)]\, (N_A/N_B) \tag{6.8}$$

The coefficient in square brackets is known as the ***k*-factor** of element A relative to element B. Although it is possible to *calculate* this *k*-factor from tabulated ionization cross sections and fluorescence yields, a more accurate value is obtained by *measuring* the peak-intensity ratio (N_A/N_B) in a spectrum recorded from a "standard" sample (such as a binary compound) whose concentration ratio (n_A/n_B) is known. This measured *k*-factor will also include any difference in collection efficiency between element A and element B (due to different absorption of x-rays in the detector window, for example).

The use of standards is common in analytical chemistry. But because the *k*-factor method was developed by metallurgists, the concentration ratio in Eq. (6.8) usually represents a *weight* ratio of two elements, rather than the *atomic* ratio n_A/n_B, and *k*-factors reflect this convention. Such *k*-factors have been measured and tabulated for most elements but their precise values

depend on the electron energy and detector design, so they are best measured using the *same* TEM/XEDS system as used for microanalysis. By analyzing characteristic peaks in pairs, the ratios of all elements in a multi-element specimen can be obtained from the measured peak integrals, knowing the appropriate *k*-factors. For further details, see Williams and Carter (1996).

6.5 Quantitative Analysis in the SEM

In an SEM, electrons enter a thick specimen and penetrate a certain distance, which can exceed 1 μm (Section 5.2). Quantification is then complicated by the fact that many of the generated x-rays are absorbed before they leave the specimen. The amount of **absorption** depends on the *chemical composition* of the specimen, which is generally unknown (otherwise there is no need for microanalysis). However, x-ray absorption coefficients have been measured or calculated (as a function of photon energy) for all the chemical elements and are published in graphical or tabulated form. A legitimate procedure is therefore to *initially* assume *no* absorption of x-ray photons, by employing a procedure based on Eq. (6.8) to estimate the ratios of *all* of the elements in the specimen, then to use these ratios to estimate the x-ray absorption that *ought to* have occurred in the specimen. Correcting the measured intensities for absorption leads to a *revised* chemical composition, which can then be used to calculate absorption more accurately, and so on. After performing several cycles of this *iterative* procedure, the calculated elemental ratios should converge toward their true values.

Another complication is x-ray **fluorescence**, a process in which x-ray photons are absorbed but generate photons of lower energy. These lower-energy photons can contribute spurious intensity to a characteristic peak, changing the measured elemental ratio. Again, the effect can be calculated, but only if the chemical composition of the specimen is known. The solution is therefore to include fluorescence corrections, as well as absorption, in the iterative process described above. Because the ionization cross sections and yields are *Z*-dependent, the whole procedure is known as **ZAF correction** (making allowance for atomic number, absorption, and fluorescence) and is carried out by running a ZAF program on the computer that handles the acquisition and display of the x-ray emission spectrum.

REFERENCE STANDARDS FOR X-RAY MICROANALYSIS

Registered Standard No. 7490

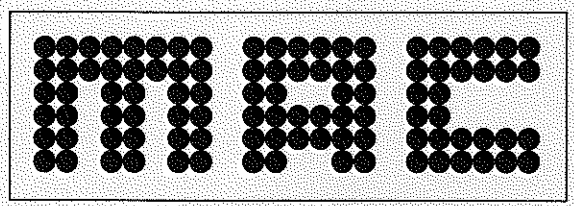

Micro-Analysis Consultants Limited

Unit 19, Edison Road, St Ives Industrial Estate
St Ives, Cambridgeshire PE27 3LF, UK
Telephone: 01480 462626 Fax: 01480 462901
email: standards@dial.pipex.com
http://www.macstandards.co.uk/town/street/yr49/

CARE OF MICRO-ANALYTICAL STANDARDS

When the standards are ready for shipment they have been through a series of rigorous checks. The final polished finish is produced through a series of diamond polishes, ending with a 1/4 micron finish. The standards are then coated with approximately 250 angstroms of carbon. The surface should not be interfered with in anyway, but if any dust should be present it should be removed using a gentle air jet.

The standards materials are mounted in a resin for its suitability to:

1) Affixing the standards in position

2) Must harden without blow holes.

3) Must withstand s vacuum and not burn readily under the action of the electron beam.

The customer should never attempt cleaning of the standards or removing the carbon film. The surface is polished to such a high degree that rubbing with the softest of tissue can damage it. Only recognised cleaning agents such as Evolve CH15 should be used if it is felt necessary and should be carried out by a qualified technician.

ON NO ACCOUNT SHOULD THE STANDARDS BE SUBJECTED TO ULTRASONIC CLEANING AS THIS IS TOO RIGOROUS AN ACTION

Micro-Analysis Consultants cannot accept responsibility for misuse of the standards by the customer. If in doubt the customer should contact M.A.C. for assistance. At all times they should be kept under vacuum or in a dessicator. Your standards were carefully packed with silica gel to keep moisture at bay and the containers were sealed in such a way that no dust should get onto the surface.

The guarantee of the standards concerns the fact that they are the materials stated and that the standards are as requested - of known composition - homogenous and suitable for microprobe analysis.

Micro-Analysis Consultants Ltd.

QCT/A Calibration Block Layout.
Block size: 32mm x 8mm Brass.

Customer Name/Order number: WWU Muenster/87001
Registered Standard number: 7490

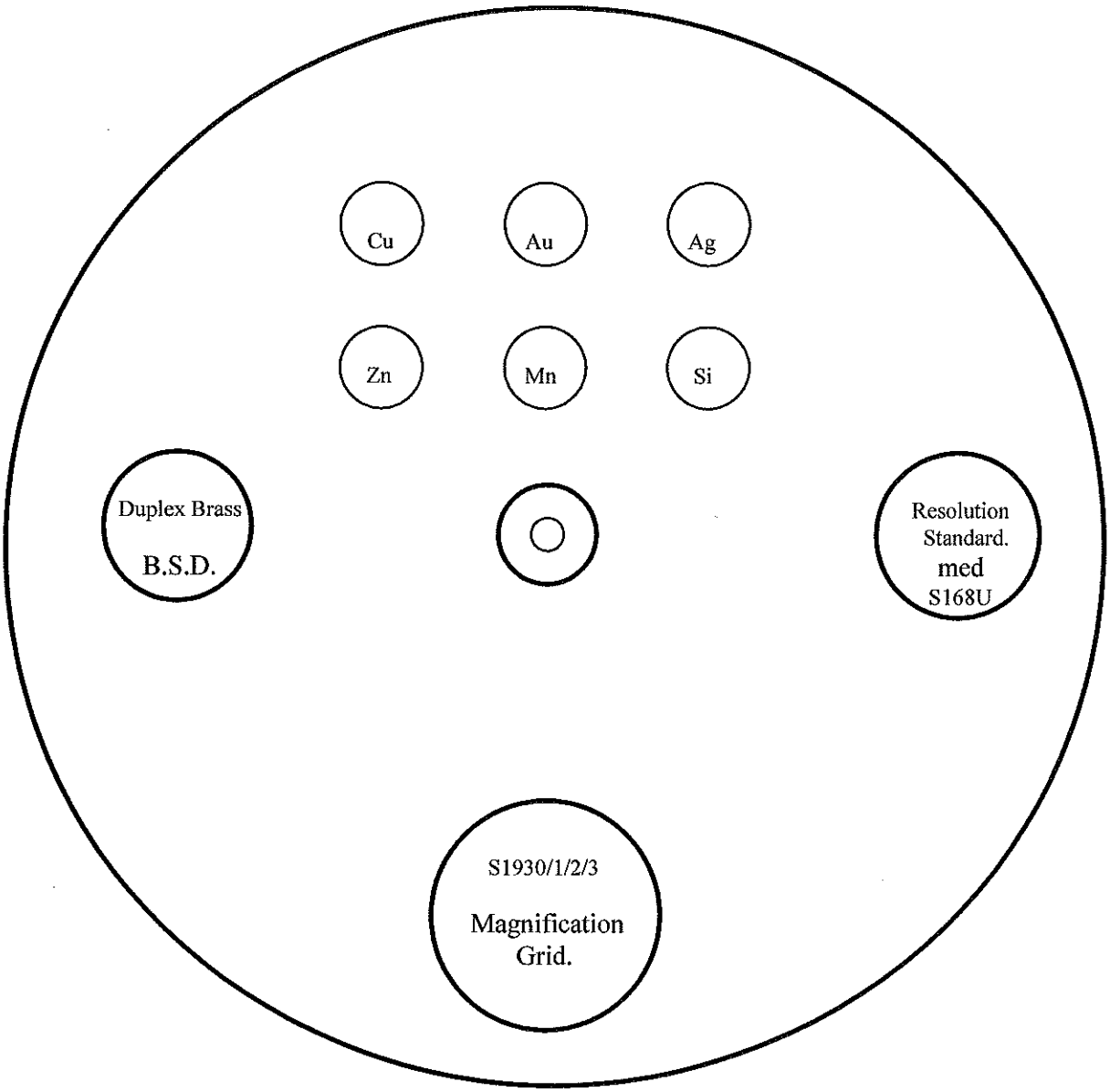

Unit 19 Edison Road, St Ives Industrial Estate
St Ives, Cambridgeshire PE27 3LF, UK.
Telephone: + 44 (0)1480 462626
Fax: + 44 (0)1480 462901

24 September 2007.

Version 2.0

Micro-Analysis Consultants Ltd.

Analysis Certificate.

Lot # 096255LN

Product #: 26612-4

Material Copper, Wire, 1.0mm diam., 99.999%

Formula: Cu **Formula Weight : 63.54**

APPEARANCE **COPPER COLORED WIRE, 1.0MM DIAMETER**

Trace Analysis:

Fe	6	ppm
Ca	2	ppm
Mg	0.1	ppm
Cu	Remainder	

Trace Metallic Impurity Analysis, ICP:

Start date:	23/11/99
Block #:	4732
Signed:	NT
Checked by:	GW
Date:	25/11/99

Unit 19, Edison Road, St Ives Industrial Estate
St Ives, Cambridgeshire PE17 4LF, UK.
Telephone: + 44 (0)1480 462626
Fax: + 44 (0)1480 462901
e-mail: standards@dial.pipex.com

Micro-Analysis Consultants Ltd.

Analysis Certificate.

Lot No: G06S014
Stock No: 14725

MATERIAL: Gold Wire, 0.5mm (0.02in) dia (Au)
Premion®, 99.999% (metals basis)

Analysis

Cu	2	Ag	1	Pt	ND
Pd	ND	Al	ND	B	ND
Fe	1	Mg	ND	Ni	ND
Pb	ND	Sn	1	Cr	1
Ge	1	As	ND	Zn	ND
Zr	ND	Si	ND	Ti	ND

Values given in ppm unless otherwise noted
ND: Not detected

Start date:	13/08/08
Block #:	7348
Signed:	CL
Checked by:	NT
Date:	13/08/08

Unit 19, Edison Road, St Ives Industrial Estate
St Ives, Cambridgeshire PE27 3LF, UK.
Telephone: + 44 (0)1480 462626
Fax: + 44 (0)1480 462901
e-mail: standards@dial.pipex.com

Micro-Analysis Consultants Ltd.

Analysis Certificate.

Lot # 11308JG

Material: Silver Ag. Wire 0.5mm dia. (Ag)

Silver. 99.99+%

Analytical Data:

Appearance: Silvery wire.

Trace Metallic Impurity Analysis, ICP:

Cu	60	ppm
Ga	10	ppm
Fe	9	ppm
Cd	2	ppm
Mg	0.4	ppm
Remainder Ag		

Start date:	6/7/00
Block #:	4889
Signed:	G Taylor
Checked by:	G Taylor
Date:	11/7/00

Unit 19, Edison Road, St Ives Industrial Estate
St Ives, Cambridgeshire PE27 3LF, UK.
Telephone: + 44 (0)1480 462626
Fax: + 44 (0)1480 462901
e-mail: standards@dial.pipex.com

Micro-Analysis Consultants Ltd.

Analysis Certificate.

Material: Zinc (Zn)

99.999% purity
6 ppm

Unit 19, Edison Road, St Ives Industrial Estate
St Ives, Cambridgeshire PE27 3LF, UK.
Telephone: + 44 (0)1480 462626
Fax: + 44 (0)1480 462901
e-mail: standards@dial.pipex.com

Micro-Analysis Consultants Ltd.

Analysis Certificate.

Stock No 36221
Lot Number 185653D1

Material Manganese pieces, irregular, 99.99% (metal Basis)

Analysis in % unless otherwise indicated.

Calcium	<0.001	Magnesium	0.001
Silicon	<0.001		

Start date:	20/11/01
Block #:	5240
Signed:	GT
Checked by:	GT
Date:	23/11/01

Unit 19, Edison Road, St Ives Industrial Estate
St Ives, Cambridgeshire PE27 3LF, UK.
Telephone: + 44 (0)1480 462626
Fax: + 44 (0)1480 462901
e-mail: standards@dial.pipex.com

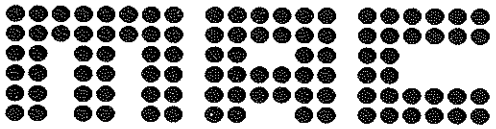

Micro-Analysis Consultants Ltd.

Analysis Certificate.

Typical analysis

Material Silicon (Si) Single Crystal

Purity: 99.999% pure (metal basis)

Unit 19, Edison Road, St Ives Industrial Estate
St Ives, Cambridgeshire PE27 3LF, UK.
Telephone: + 44 (0)1480 462626
Fax: + 44 (0)1480 462901
e-mail: standards@dial.pipex.com

Micro-Analysis Consultants Ltd.

Analysis Certificate.

Certified Reference Material Information

Type: MAJOR ELEMENTS IN BRASS (CHILL CAST)

Form and Size: Disc 42mm Diameter x 18mm Thickness

Certified Analysis

Percentage element by weight

Elements and Values

Sn	0.151	Pb	0.0129	Zn	39.57	Fe	0.0191
Ni	0.0124	Al	0.0172	Mn	0.0249	Si	(0.0072)
Cu	60.13	Co	(0.0002)	As	0.0222	Bi	0.0107
Sb	0.0207	B	0.0056				

Unit 19, Edison Road, St Ives Industrial Estate
St Ives, Cambridgeshire PE27 3LF, UK.
Telephone: + 44 (0)1480 462626
Fax: + 44 (0)1480 462901
e-mail: standards@dial.pipex.com

Agar SCIENTIFIC

Technical Information

AGAR GOLD ON CARBON SEM CALIBRATION SPECIMEN

S168, S168A, S168B, S168C, S168D, S168E, S168T, S168U

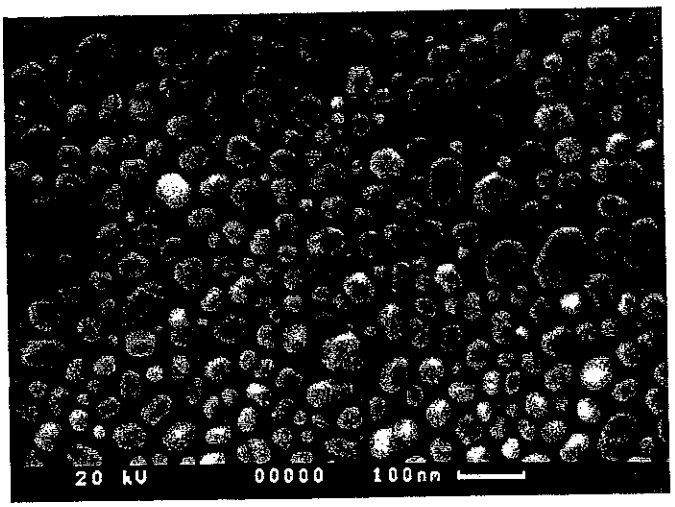

General Information

This calibration specimen provides a means of testing scanning electron micro-scopes. It supersedes the previous two types of specimen offered by Agar Scientific since it shows both large and small gaps. The various sizes of the gaps between gold crystals grown on a graphite substrate allow tests for the resolution attainable under real operating conditions: concomitantly, the samples can be used to assess the quality of grey-level reproduction at high resolution. Ideally, high resolution scanning microscopes should give good results in the gap test combined with good grey level reproduction. Medium-quality instruments may achieve a chosen gap resolution, but the grey-level production may be quite poor, for example, only 4 or 5 grey levels may appear. Grey levels arise in the secondary electron mode due to differential signal collection and this originates from geometric irregularities on the test specimen. Hence, the angular crystal faces in the larger gold crystals in this specimen can be used for the grey level assessment.

As an aid in use, there is an outline image of a square mesh on the surface of the specimen: this is useful for preliminary focusing at magnifications below x150. In addition, if the user wishes to preserve the specimen then tests can be done on known areas leaving other areas unirradiated. For a demanding assessment of the imaging qualities of the microscope, the microscopist may wish to view the very fine array of particles present in the boundary region between evaporated gold in the grid squares and uncoated graphite in the grid bars.

When assessing the secondary electron image quality, the sample is best viewed using a specimen tilt of 30 degrees to the secondary electron collector. The degree of stage tilt used in back-scattered electron testing will depend on the position of the detector. It is better not to view the sample in any mode with a tilt greater than 35 degrees since the height of the larger crystals may be such that the small crystals become shielded from view.

If gap measurements are to be made it should be remembered that the magnification is not constant throughout the image when the sample is tilted.

Agar Scientific Limited, 66a Cambridge Road, Stansted, Essex CM24 8DA, England
Tel: +44(0)1279 813519 Fax: +44(0)1279 815106 e-mail: sales@agarscientific.com www.agarscientific.com Registered in England No. 1601520

Using The Specimens

1. Setting up the SEM

The gold crystals are difficult to visualise on the VDU when the SEM is working below x 40,000 magnification. Other than giving this simple comment, recommending conditions for SEM resolution and grey level testing is somewhat difficult since there are many levels of sophistication available in the current generation of instruments. As a general guide, the operator will be aiming to use the test specimen at a fairly short working distance of 7 or 8mm. The best probe sizes are available at higher probe energies, so a gun potential of 20kV or above should be chosen for the initial testing. Subsequently it may be of interest to examine the performance of the SEM at lower gun potentials: however, unless the SEM in question has a dedicated facility for high quality imaging at below 10keV, there will not be much point in attempting work at this level. It is important that the filament is correctly saturated and that the gun is working efficiently in terms of beam brightness and stability, that the apertures are carefully centred, and that the astigmatism and fine focus are carefully checked immediately prior to recording the image. For ultimate performance the stage should be mechanically stable, there should be a good chamber vacuum, and the stray field and ambient vibration level in the SEM room should be below the recommended level set by the SEM manufacturer. For recording, if the variables are available, the largest number of scan lines per frame resolvable on the recording screen should be used, and a long recording time is recommended (up to 10 minutes may be available on some instruments) which should ensure a good signal to noise ratio. If the operator is looking for good grey level reproduction, it is very important that the recording camera lens is well focused and that the photographic processing is carefully controlled for the best grey range available. Measurements of gaps can of course only be made after a careful magnification calibration of the SEM, and the microscopist must be satisfied that the calibration is rigorously applicable to the micrograph recorded of the Au/C test specimen.

2. A Suggested Imaging Strategy

Set up the SEM then insert the sample and await a good vacuum. Switch on the gun and saturate the filament carefully. Starting at a low magnification (below x150), focus on the edges of the dark grid bars and search for a suitable square of gold. Raise the magnification to x500 and focus on an irregular portion of the gold film. Increase the magnification to x40,000 keeping the specimen in focus. Shift the specimen to image an area well within a grid square (if the stage is tilted, use X-shift for convenience so that you do not lose focus): now focus carefully on the gold particles. Raise the magnification to x80000 (or above) and make final adjustments to the stigmators and the fine-focus controls. The latter adjustments should be performed quickly if the SEM is prone to contamination deposition. Record the image using a very slow probe scanning rate.

Re-ordering Information:

S168	Au-C test specimen on 12.5mm pin stub.
S168A	Au-C test specimen on JEOL stub.
S168B	Au-C test specimen on ISI stub.
S168C	Au-C test specimen on Hitachi stub.
S168D	Au-C test specimen on customer's stub.
S168E	Au-C test specimen on 12.5mm x 10mm stub
S168T	Au-C test specimen on thin carbon
S168U	Au-C test specimen - unmounted

Ultra High Resolution Calibration Specimens are also available:

S1969	Particle size range < 2nm-30nm
S1987	Particle size range < 3nm-50nm

Agar SCIENTIFIC

PLANOTEC SILICON TEST SPECIMEN

S1930/1/2/3

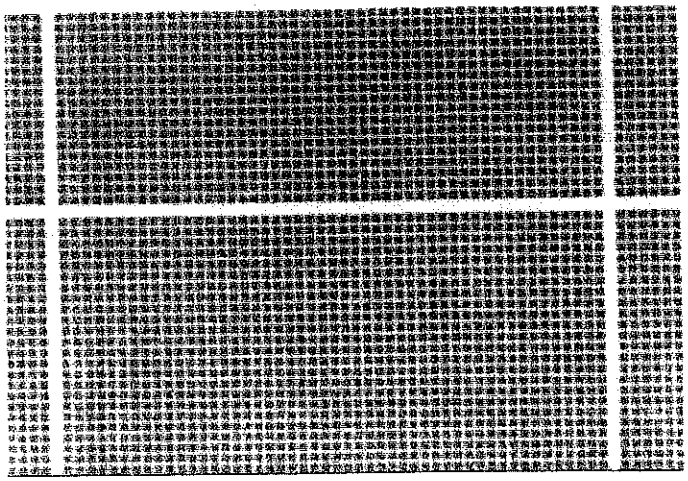

The test specimen consists of lines etched into a single crystal silicon substrate. They have been written by electron beam machinery, and consist of a square mesh of course lines of 500μm spacing with 50 intermediate fine lines of 10μm spacing.

The 10μm pitch has been measured using an automatic line width measuring system. The measurements obtained from wafer number GFN 024-MI below:-

Position	Pitch measurement μm
1	10.020
2	10.050
3	10.050
4	10.050
5	10.090
6	10.020
7	10.090
8	10.090
9	10.010

Max	10.100
Min	10.020
Mean	10.062
3 Sigma	0.088

Agar Scientific Limited, 66a Cambridge Road, Stansted, Essex CM24 8DA, England
Tel: +44(0)1279 813519 Fax: +44(0)1279 815106 e-mail: sales@agarscientific.com www.agarscientific.com Registered in England No. 1601520

Final Inspection and Test.

Customer/Order number: WWU Muenster/87001

	Checked by	Date	Pass	Fail	Comments
Standard # 7490	[illegible]	5-1-09	✓		
Optical Inspection	[illegible]	5-1-09	✓		
Electron Optical Inspection	[illegible]	5-1-09	✓		
X-Ray Analysis	[illegible]	5-1-09	✓		
Accepted	[illegible]	5-1-09			
Rejected					

☑ 1) We recommend that you return the standards two years from the above date for further re-polishing.
☐ 2) It is recommended that these standards are not suitable for further re-polishing.